coatings

MDPI

Article

Effects of Mechanical Activation on Physical and Chemical Characteristics of Coal-Gasification Slag

Feng Wu [1,2], Hui Li [1,2,*] and Kang Yang [1,2]

[1] College of Materials Science and Engineering, Xi'an University of Architecture and Technology, Xi'an 710055, China; wufeng@xauat.edu.cn (F.W.); yangkang@xauat.edu.cn (K.Y.)
[2] State Key Laboratory of Green Building in Western China, Xi'an University of Architecture and Technology, Xi'an 710055, China
* Correspondence: sunshineli@vip.sina.com

Abstract: Coal-gasification slag (CGS) was subjected to mechanical grinding by three different methods. We studied the effects of mechanical activation on various physical and chemical characteristics of the CGS, including particle-size distribution, specific surface area, mineral composition, degree of crystallinity, particle morphology, chemical bonding, surface activity and binding energy, anionic-polymerization degree and hydration properties. The results show that there are different effects on CGS characteristics depending on the type of activation applied. Mechanical activation also can increase the specific surface area and the dissolution rates of activated SiO_2 and Al_2O_3, and the major elements (O, Si, Al, Ca) in CGS, whereas the degree of crystallinity and of polymerization of $[SiO_4]$ and $[AlO_6]$ are reduced by mechanical activation. We also found that the effects of different mechanical-activation methods on the compressive strength and activity were similar and could accelerate the hydration process.

Keywords: mechanochemical activation; coal-gasification slag; particle characteristics; cementitious material; reactivity

Citation: Wu, F.; Li, H.; Yang, K. Effects of Mechanical Activation on Physical and Chemical Characteristics of Coal-Gasification Slag. *Coatings* **2021**, *11*, 902. https://doi.org/10.3390/coatings11080902

Academic Editors: Andrea Nobili, Filippo Berto and Frederic Sanchette

Received: 26 May 2021
Accepted: 20 July 2021
Published: 28 July 2021

1. Introduction

In recent years, coal-gasification technology (CGT)—such as used by Texaco, Shell and Grup Servicii Petroliere—has become one of the leading clean coal technologies. A new technology, CGT can not only make the coal attain high value-added utilization, but it also will not produce sulfur dioxide, carbon dioxide and other harmful gases [1,2]. Thus, it effectively supports environmental protection. Coal-gasification slag (CGS), a byproduct of CGT, could reduce the advantages of the CGT as a clean technology [3,4]. To highlight the advantages of CGT, such as 'zero emissions', the environmental safety problems of CGT byproducts must be addressed and all-encompassing solutions developed and sustainable development achieved [5,6]. There are two types of CGS, fine-grained and coarse-grained. The fine-grained slag, 10% of the total CGS output, has a relatively high carbon content (as high as 15–30%) [7]. Inhomogeneous and porous, it can be used as an adsorbent to purify water. The coarse-grained slag, 90% of the total CGS output, has a relatively low carbon content and is dense, hard, inhomogeneous and amorphous [8]. It has many uses, such as a polishing compound, a cement additive, a component of concrete aggregate and road-surface coating [5,7,9–11].

As is widely known, much of the CGS produced by CGT has been harmful to the local ecological environment. Due to similar serious environmental problems are known to have been caused by CGS abroad (such as in Spain, Poland and Japan), a lot of research on uses of CGS has been carried out [12–17]. They found that the CGS could be used to fabricate building bricks, but the mechanical properties of such bricks could be improved. They also confirmed the potential for lightweight aggregates by using integrated-gasification combined cycle slag and demonstrated that their properties rivalled

those of existing commercial lightweight aggregates. In China, gasification slags have been used mostly in civil construction such as raw materials for pavement or building bricks and pavement-base/subbase [18–22]. However, these research results do not make full use of the cementitious characteristics of CGS.

It is also well known that the physical and chemical characteristics of CGS determine its suitability for various uses [23]. Mechanical activation is a method that can induce a series of physical and chemical changes in solid materials by applying shear, compression, impact, bending and extension, which also induce solid–liquid, solid–gas and solid–solid chemical reactions [24]. In the process of mechanical grinding, the structure of solid materials will be greatly changed: The particle size of inorganic nonmetallic materials will be rapidly refined, the surface area of particles will rapidly increase, crystal-lattice distortion will occur and lattice defects will be produced and the amorphous (non-crystalline) character will be intensified [25,26]. At the same time, the chemical activity will increase, and the reaction conditions between inorganic nonmetallic materials and other materials will be reduced, thus resulting in the so-called mechanization-learning effect [27,28]. In the process of mechanical grinding, if the chemical composition of the solid material does not change, it is called mechanical activation, but if the chemical composition or structure of the solid material also changes, it is called mechanochemical activation [29,30]. Under the action of mechanochemistry, solid materials have more active points per unit mass, which can greatly improve the reactivity; it has been used widely in practical applications [31]. In addition, the most commonly used mechanical activation instruments in the laboratory are ball mill, vibration mill and prototype machine. However, there are few experimental studies about improving activity by mechanical activation, the effect of mechanical-activation methods on basic physical and chemical CGS properties. Too, the reaction mechanism of preparing cementitious materials from CGS have not been reported [32,33].

As CGS is generally coarse-grained, reactivity is minimal without grinding. In this study, we focused our research on CGS produced by CGT. The differences in physical and chemical characteristics of CGS subjected to various mechanical activations were analyzed from different perspectives, such as particle-size distribution, mineral composition, degree of crystallinity, particle morphology, chemical bond, surface activity and binding energy, anionic-polymerization degree and hydration properties. To understand the physical and chemical changes induced by various mechanical activations, the activated CGS was characterized by particle-size analysis, X-ray diffraction (XRD), scanning electron microscopy (SEM), Fourier transform infrared (FTIR) spectroscopy and X-ray photoelectron spectrometry (XPS). Furthermore, we assessed the hydration characteristics of cementitious material prepared from activated slag.

2. Raw Material and Experimental Methods

2.1. Raw Material

The CGS used in this research was provided by Shenhua Ningmei Group. It was ground to a specific surface area by applying three grinding methods: ball mills (QM), vibration mills (ZD) and a type of prototype machine (ZY), ZY is a kind of small equipment similar to the refiner, it is ground by friction and rubbing between the rotating disc and the material. The yielded average particle sizes of ~20 μm and ~7 μm, respectively. Cement, provided by Sheng wei cement company, had a specific surface area of 370 m^2/kg. The chemical composition of the CGS and of the cement are shown in Table 1, and a photomicrograph of the CGS is shown in Figure 1.

Table 1. Composition of Coal-gasification Slag and Cement.

Composition	SiO_2	Al_2O_3	CaO	Fe_2O_3	MgO	Na_2O	K_2O	P_2O_5	SO_3	Other	LOI
CGS	48.75	20.05	10.69	9.67	2.84	1.65	2.11	0.17	0.56	1.88	1.52
Cement	18.21	3.37	64.59	2.88	3.89	0.51	1.02	0.48	1.37	0.48	3.19

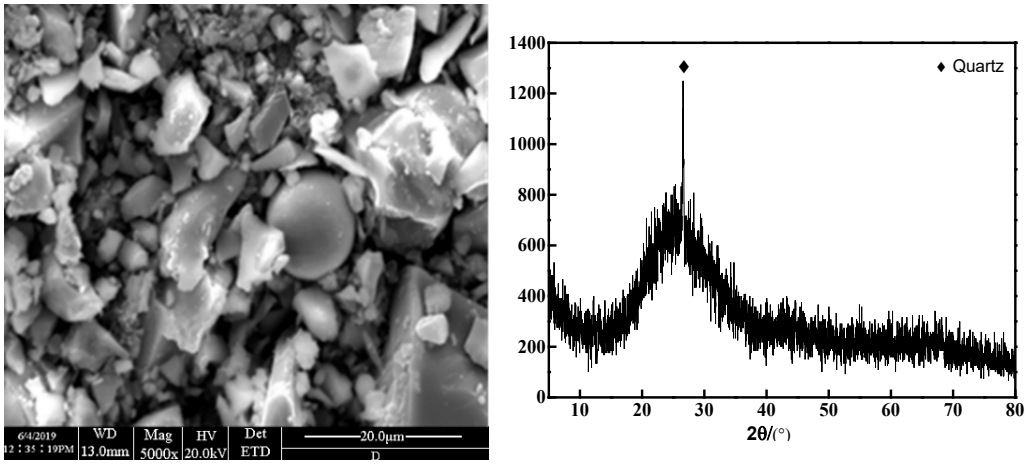

Figure 1. Microscopic morphology (**a**) and mineral components (**b**) of coal-gasification slag.

The CGS contains mainly silica (SiO_2), aluminum oxide (Al_2O_3), calcium oxide (CaO) and iron oxide (Fe_2O_3) with small amounts of various RO and R_2O phases; the total content of SiO_2, Al_2O_3 and CaO is >70%, and the loss on ignition is 1.52%. The CGS is characterized by heterogeneous morphology; its irregular forms include flakes and rods, and a small amount of spherical particles form an included powder. The surface of the particles is very dense, and CGS porosity is low. The CGS contains mainly an amorphous glass phase and small amounts of silica (quartz phase). The relatively high glass-phase content is favorable for the dissolution of the activated SiO_2 and Al_2O_3.

2.2. Mechanical-Activation-Material Sample Preparation

CGS grinding experiments were carried out by using the three methods QM (Φ 300 mm × 300 mm), ZD (MZS-3 in laboratory) and ZY (a type of prototype machine), resulting in particle sizes of ~20 um and ~7 um, respectively, all the grinding methods are dry grinding. When the QM was used for grinding and using the most compact packing theory to match the ball, the grinding material was steel ball, the ratio of ball to material was 10:1. When the ZD was used for grinding, the grinding material was steel ball, the grinding material was zirconia ball, and the ratio of ball to material was 10:1, the filling rate of zirconia ball was 80%. There are three particle sizes of zirconia ball: Φ 5 mm, Φ 10 mm and Φ 15 mm, the total weight of zirconia balls was 6.0 kg, and the ratio was 3:5:7. When the ZY was used for grinding, the addition amount of coal gasification slag was 60 g.

2.3. Experimental Methods

1. The mineral composition of the activated CGS was analyzed by XRD, the X-ray diffraction method (D/max 2200, Rigakul Corporation, Tokyo, Japan). The measuring speed was at 10° (2θ)/min in the 2θ range of 5–75°. the chemical composition was measured by X-ray fluorescence (XRF, Brooke Instruments Co., Ltd., Brooke, Germany), the particle morphology of the activated slag was observed by SEM (FEI Company, Oregon, OR, USA), the anionic-polymerization degree of the CGS was analyzed by FTIR (Shimadzu Corporation, Kyoto, Tokyo), and the surface activity and elements were analyzed by chemical analysis and XPS (Rigakul Corporation, Tokyo, Japan).
2. The CGS paste was prepared as follows: First, it was prepared from 70 wt% cement and 30 wt% CGS, resulting in a water–binder ratio of 0.5 for the paste. The specimens were cured at 20 ± 1 °C and >95% humidity for 3 d, 7 d and 28 d, respectively. Then the strength of CGS was measured according to Chinese National Standard GB/T17671-1999.
3. We used three types of equipment to grind CGS in this study: ball and vibration mills and a prototype machine. During the grinding process, CGS underwent a series

of physical and chemical changes, and its microstructure also changed accordingly. Changing the structure modified the performance, thereby improving its reactivity. For each grinding mode, a parallel group was set by changing the duration of mechanical grinding to form two CGS samples, one fine-grained and one coarse-grained. The performance of the CGS of the same particle size (fine- or coarse-grained) produced by different grinding methods was compared, and the effects of different grinding methods were analyzed. The influence of CGS gelation activity and the grinding parameters of different equipment are shown in Table 2.

Table 2. Grinding Parameters.

Grinding Equipment	QM	ZD	ZY
Grinding Time	2.5 h 1 h	2 h 1 h	2 min 1 min

3. Properties of Mechanically Activated Coal-Gasification Slag

3.1. Particle-Size Distribution of Activated Slag

The particle-size distribution of CGS activated by different grinding methods was measured by a laser particle-size analyzer (Figure 2). The particle size of by different grinding methods are shown in Table 3, The CGS particle size is significantly reduced by controlled extension of the grinding time by a particular method. This may be due to the natural defects in the CGS subjected to the action of mechanical force. When the slag is being destroyed, its particle size is rapidly refined along the defect interface, showing a macroscopic decrease in particle size and an increase in specific surface area.

The particle-size and frequency distribution curves for CGS activated by the three grinding methods are similar. The particle size averages ~7 μm, and <20 μm particles account for >90%. The median particle size and volume average particle size of the CGS are similar for the three different grinding methods (QM, ZD and ZY), and their particle-size and frequency distribution curves are very similar. The particle size is concentrated mainly ~20 μm, and the particle size of >90% particles is <50 μm. Thus, it is apparent that the different grinding methods have little effect on the CGS particle-size distribution. The purpose of extending the activation time of mechanical activation is to optimize the particle size distribution of samples. Previous studies have shown that the geopolymer synthesized by the samples has a low strength value, which is closely related to the particle size distribution of samples [34].

The specific surface area of the material output by different grinding methods applied for different grinding times is shown in Table 4.

After applying any of the different grinding methods, the specific surface area of the activated slag significantly increases owing to structural damage to the material under the action of mechanical force, which leads to the reduction of particle size. Comparing the different grinding methods resulting in the same particle size, the specific surface area of the CGS produced by mechanical activation by the prototype machine is the largest, and that generated by the vibration mill is the smallest. This is caused by the different working principles of different equipment for grinding materials. However, when applying the same grinding method, the specific surface area of the material increases significantly with the extension of grinding time. This phenomenon is related to the particle-size distribution of the material, to which in turn the change in surface area corresponds [35]. With the appropriate increase in grinding time, the material particle size decreases and its specific surface area increases, and the phase composition will change.

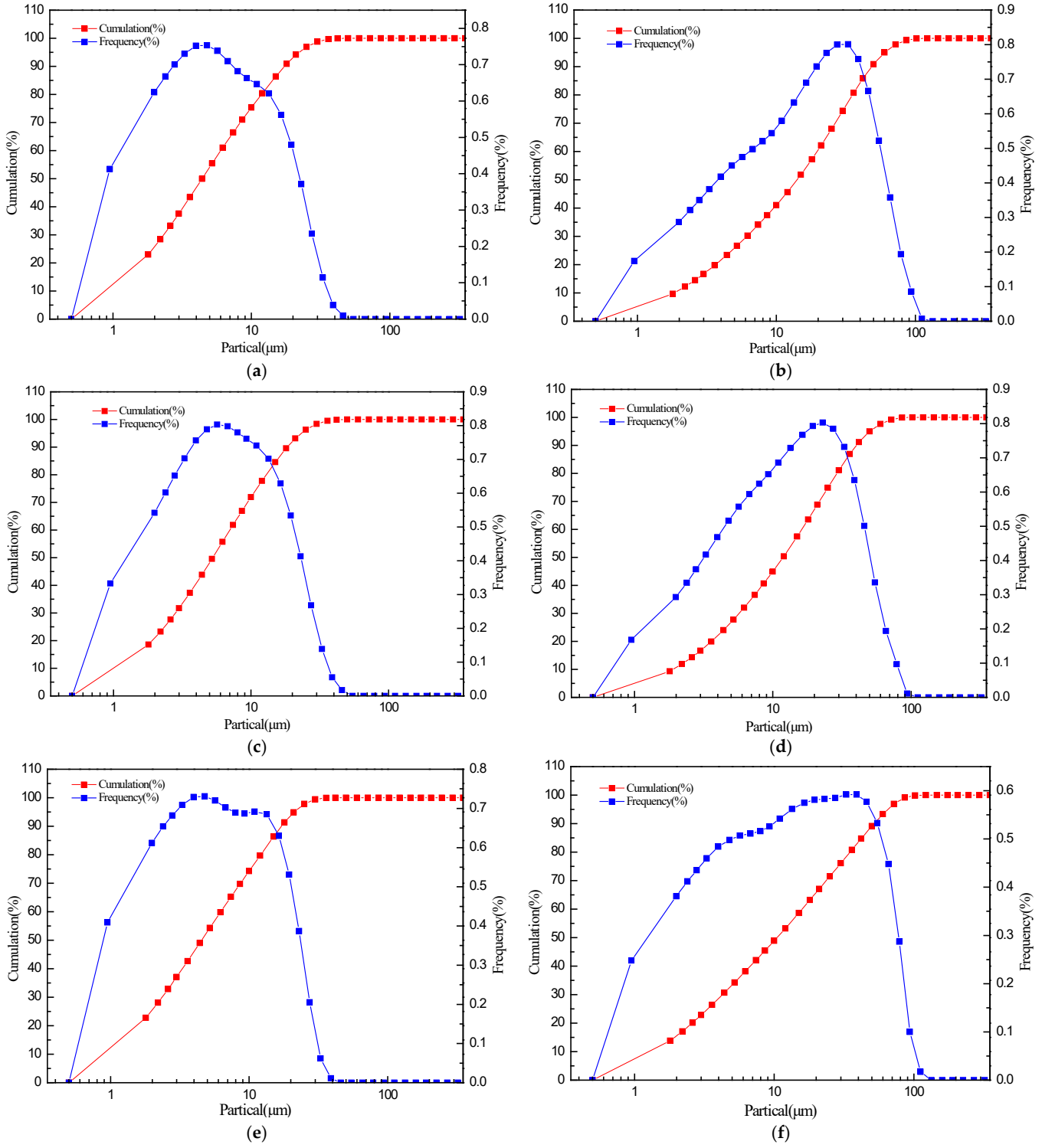

Figure 2. Influence of different mechanical-activation methods on powder particle-size distribution. (**a**) QM-2.5 h; (**b**) QM-1 h; (**c**) ZD-2 h; (**d**) ZD-1 h; (**e**) ZY-2 min; (**f**) ZY-1 min. (QM, ball milling; ZD, vibration mill; ZY, prototype machine.).

Table 3. Characteristic Particle Size of Activated Slag.

Grinding Method	**QM**		**ZD**		**ZY**	
Grinding Time	2.5 h	1 h	2 h	1 h	2 min	1 min
Median Particle Size D_{50} (μm)	5.41	14.25	5.27	11.86	4.55	10.52
D_{90} (μm)	18.40	48.66	18.36	40.35	17.20	52.04
Average Diameter (μm)	8.79	19.84	7.74	17.17	7.08	19.28

Table 4. Specific Surface Area of Activated Slag.

Grinding Method	**QM**		**ZD**		**ZY**	
Grinding Time	2.5 h	1 h	2 h	1 h	2 min	1 min
Specific Surface Area (m^2/kg)	864.55	471.29	703.77	409.55	921.20	671.56

3.2. Mineral-Composition Analysis

The diffraction pattern of the cinder (Figure 3) is a disordered pattern. With no obvious crystal peak, it represents mainly amorphous material. The mechanochemical effect of the CGS was produced by different mechanical treatments. A narrow and sharp crystal peak and a non-crystal (amorphous) bulge peak are apparent at 20~30° (2θ); the crystal peak represented the quartz phase, produced by all three methods in a short grinding time. In contrast, a crystal peak at 47° represents an iron phase that appeared in the ball-milling diffraction pattern but was not produced by the other two methods. This may be due to the mechanical damage to the CGS structure, particle-size reduction, being encased in the inner quartz-crystal structure later exposed, or the formation of the iron phase may be due to the extrusion, impact and collision between grinding balls, which results in the mixing of some iron phases in the powder. With increased grinding time, the intensity of the diffraction peak of the original crystal decreases, the intensity of the amorphous bulge peak increases, and the diffraction peak is more diffused. With the simultaneous quartz-crystal-lattice distortion, the structure changes to amorphous as the crystallinity of the slag decreases, the inert glass structure depolymerizes and the dissolution rate of active Si and Al in the CGS increases.

It is known that mechanical activation can cause the reduction in crystallinity degree of mineral phases, i.e., and active sites increase in the amorphous content. The transformation of crystalline material into amorphous enhances its reactivity. Mechanical activation influenced enhanced availability of activated SiO_2 and Al_2O_3 during the process of geopolymerization [36,37].

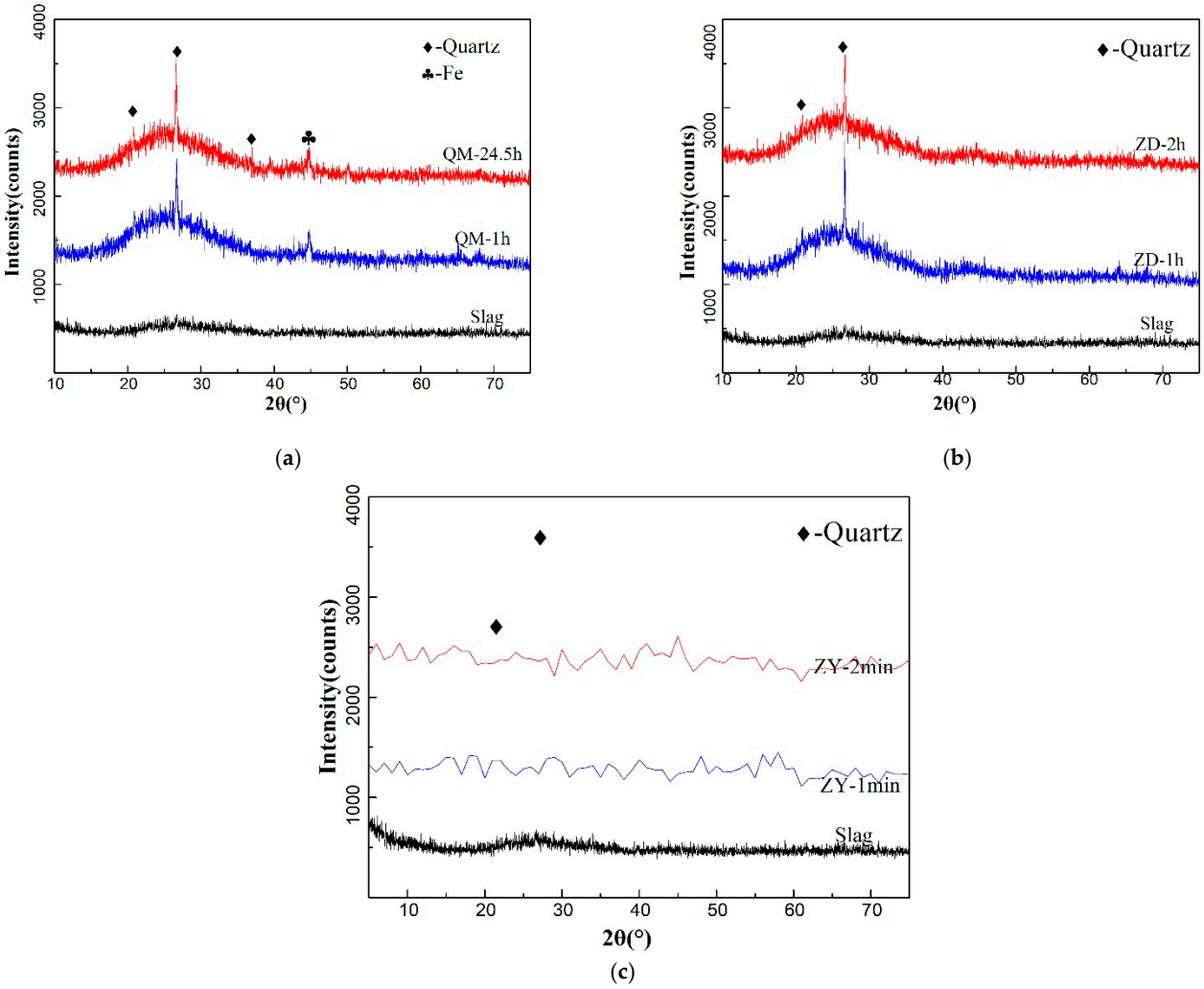

Figure 3. Mineral composition of slag produced by different mechanical-activation methods. (**a**) QM; (**b**) ZD; (**c**) ZY.

3.3. Particle Morphology

CGS micromorphology has changed greatly after being ground by various grinding equipment. Under the action of mechanical force, spherical particles and dense irregular larger particles form sheetlike or blocklike configurations to varying degrees; the particles are rapidly ground finer, the original spherical particles giving way to compact irregularly shaped particles with sharp edges and corners and showing good dispersion [37].

By comparing the output from the same grinding method at different grinding times, we found that (Figure 4) over time, the irregular large particles collided and impacted each other under the action of mechanical force, whereby they were further refined into smaller irregular particles showing no evidence of the structure of the original spherical particles. A good particle-size distribution is established as a small number of large particles and a large number of small particles become thoroughly intermixed, while also a large number of spherical particles in the slag become almost invisible and a large number of irregular polygonal particles form. We also found that the CGS particles formed by ball and vibration mills have sharp edges and corners, whereas the CGS formed by the prototype sample-making machine has relatively smooth edges and corners. A photomicrograph also revealed that the particle size of the CGS sample after grinding by the prototype machine is smallest and after grinding by the vibration mill is the largest; this outcome is consistent with the specific surface area of resulting particles given different grinding methods. The sample-making machine yields the largest specific surface area, while the vibration mill yields the smallest.

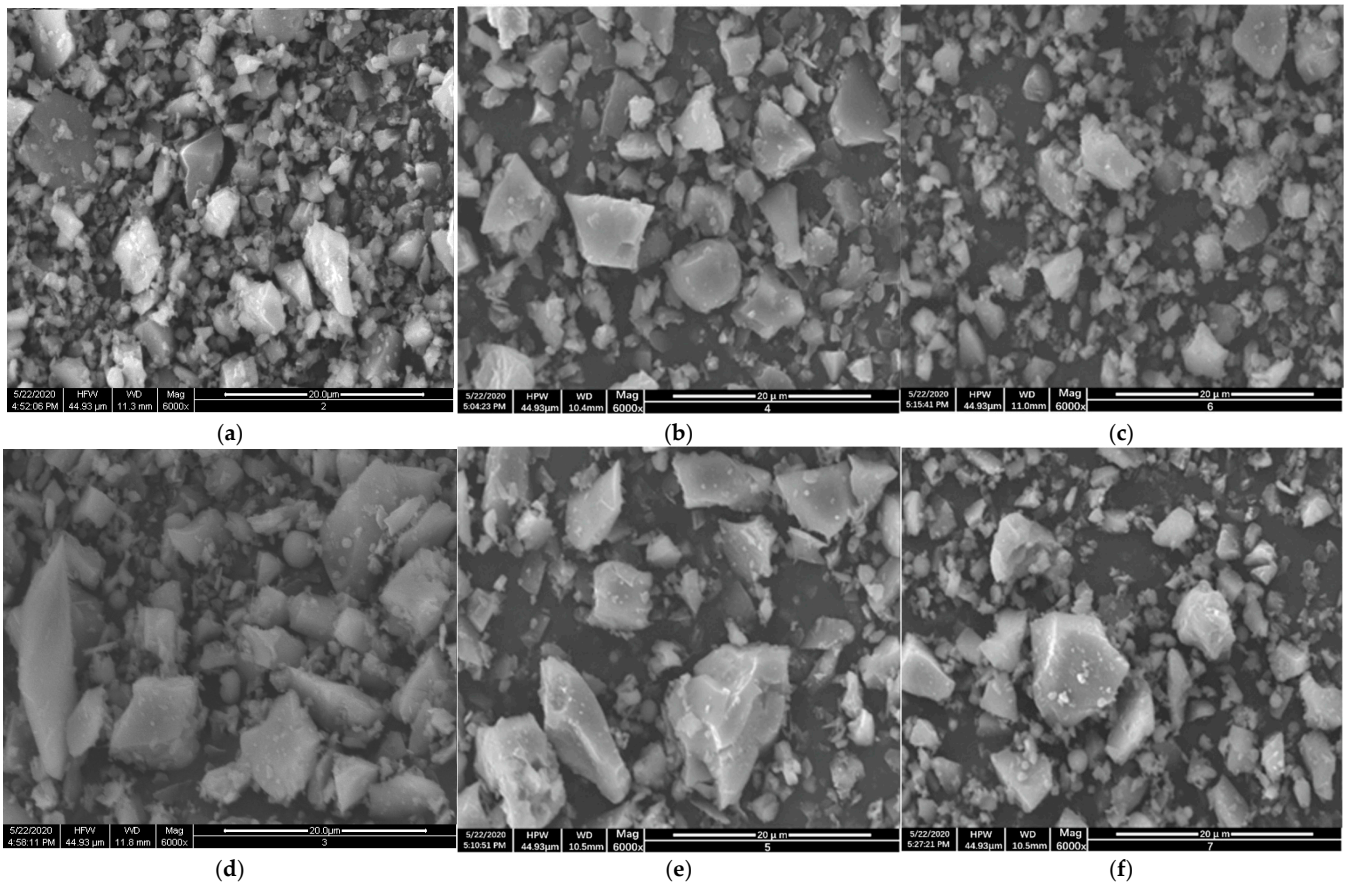

Figure 4. Photomicrograph of coal-gasification slag with different grinding methods. (**a**) QM-2.5 h; (**b**) ZD-2 h; (**c**) ZY-2 min; (**d**) QM-1 h; (**e**) ZD-1 h; (**f**) ZY-1 min.

3.4. Chemical-Bond Analysis

The CGS records changes in a physical-chemistry series under the action of mechanical force. We used FTIR to analyze the internal structural change of the CGS activated by mechanical treatment.

The presence of quartz causes a series of bands at about 1150, 1080, 796–778 (double band) and 480 cm^{-1} [38–40]. There are stretching-vibration peaks in the slag (Figure 5); the strong absorption peak at 3441 cm^{-1} and 1593 cm^{-1} are caused by stretching vibration of the O–H bond, and the absorption peak at 1380 cm^{-1} and 1352 cm^{-1} are caused by stretching vibration of C–O–C, the absorption peaks at 1087 cm^{-1} and 989 cm^{-1} are caused by the asymmetric stretching vibration of the Si–O–Si bond. The wave band at 761 cm^{-1} may be related to the symmetric stretching vibration of Si–O–Si and the AlO_4 vibration, and the absorption peak at 481 cm^{-1} is caused by the bending vibration of the Si–O–Si bond.

The FTIR spectra of CGS activated by different grinding methods are similar, and the absorption peaks of CGS activated by ball or vibration milling and by prototype-machine grinding at 1087 cm^{-1} and 989 cm^{-1} shift to lower wavenumbers to different degrees, and with the increase in grinding time, the absorption peak at 989 cm^{-1} decreases gradually until it disappears. The shift from the absorption peak to the low wavenumber can reflect the change of the structure of the silicon–oxygen tetrahedron in the activated CGS; the change of the degree of polymerization from the high to the low state leads to the increase of the content and activity of the low state vitreous. The bending vibration of the Si–O–Si bond at 481 cm^{-1} also confirms this phenomenon.

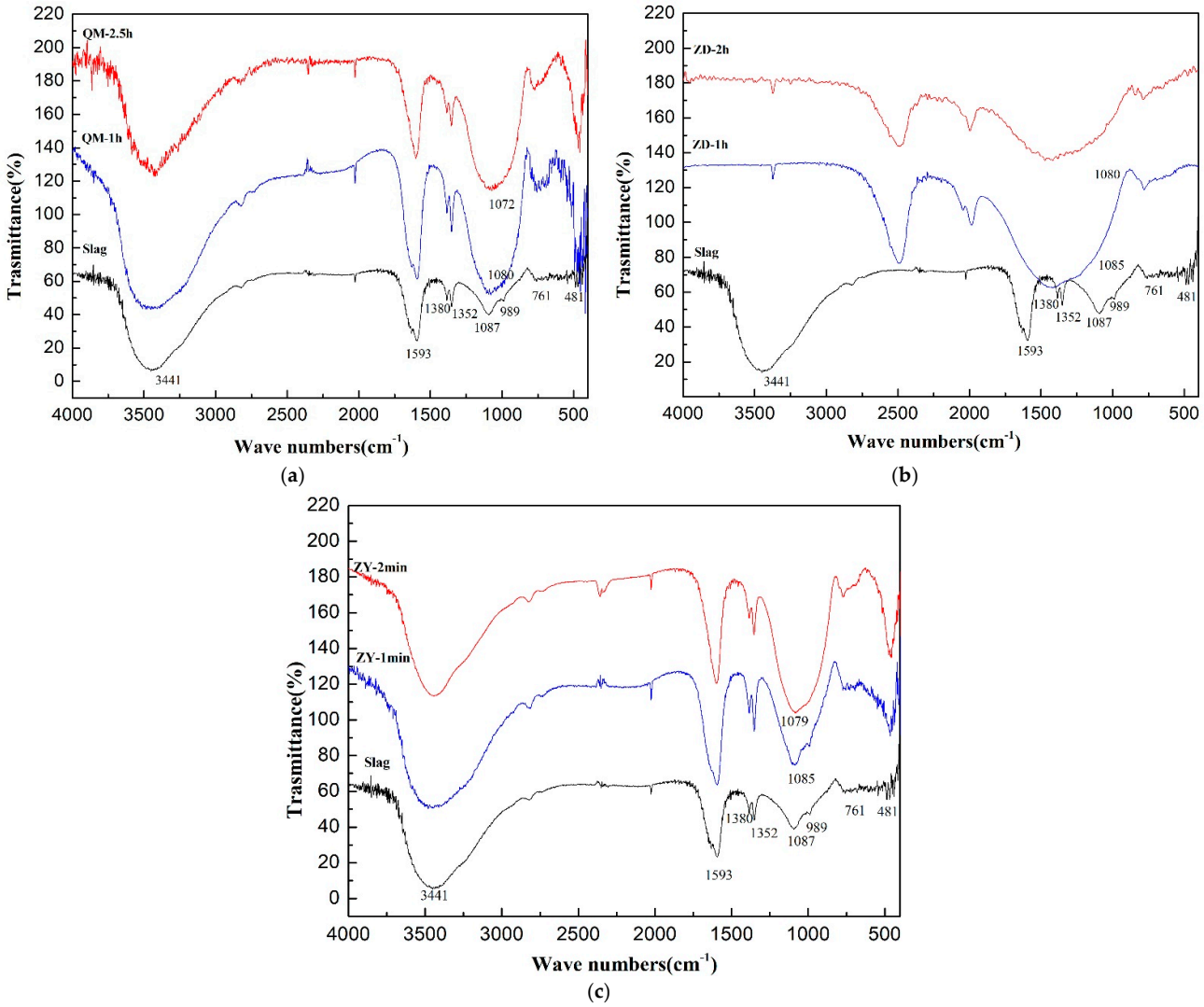

Figure 5. FTIR spectra of activated coal-gasification slag under different grinding methods. (**a**) QM; (**b**) ZD; (**c**) ZY.

Given the same grinding method, at shorter grinding times, the peak intensity of the spectral lines increases and the absorption-band intensity increases because of the quartz-crystal phase in the CGS after grinding. However, as the grinding continues, the band of the absorption spectrum becomes wider and weaker owing to the destruction of the crystal lattice and the depolymerization of the glass structure of the high polymer state. From the above analysis, it can be concluded that the CGS bond structure can be changed by using different mechanical-grinding methods; the CGS crystallinity is reduced, the structure becoming amorphous as the content of activated glass increases.

3.5. Surface-Activity Analysis

From these results (Table 5), it can be seen that three different grinding methods can effectively improve the digestion rate of activated SiO_2 and Al_2O_3 in CGS. Furthermore, the total amount of SiO_2 and Al_2O_3 in activated CGS from the use of a vibration mill or a prototype machine was similar, while the total amount of SiO_2 and Al_2O_3 dissolved from activated CGS was the lowest when ball milling was used. Given the same grinding method, the dissolution rate of active SiO_2 and Al_2O_3 increases with the increase in grinding time, because with the extension of grinding time, the mechanical force acting on the material destroys its structure, crystalline material becomes amorphous, the structure of the inert vitreous body is dispersed and depolymerized and the SiO_2 and Al_2O_3 in the amorphous mineral are separated to form active SiO_2 and Al_2O_3. With higher dissolution rates of

SiO_2 and Al_2O_3 in activated CGS, both the activity of activated SiO_2 and Al_2O_3 and the degree of participation of activated SiO_2 and Al_2O_3 as cementitious material in hydration reactions increase.

Table 5. Dissolution Rate of Activated SiO_2 and Al_2O_3 in Different Activated Coal-gasification Slags.

Grinding Mode	Dissolution Rate of Active Silicon/%	Leaching Rate of Active Aluminum/%	Total Dissolution of Silicon and Aluminum/%	Activity Rate K_a/%
CGS	6.789	3.105	9.894	14.38
QM-2.5 h	20.544	10.383	30.927	44.95
QM-1 h	15.525	7.506	23.031	33.48
ZD-2 h	19.154	11.876	31.03	45.10
ZD-1 h	16.142	8.398	24.540	35.67
ZY-2 min	21.058	11.010	32.068	46.61
ZY-1 min	15.006	9.027	24.033	34.93

3.6. Surface Binding Energy

XPS analysis was used to further understand the chemical-state changes of several typical elements in CGS particles before and after mechanochemical activation. Full-spectrum scanning indicated that the elements O, Si, Al and Ca were mainly near the surface of slag (especially in ball-milled slag). Then we applied fine-spectra scanning of O_{1s}, Si_{2p}, Al_{2p} and Ca_{2p}.

That the electron-binding energy of elements changes with mineral structure enables qualitative analysis of the structure and activity of minerals using XPS analysis (Figure 6). By analyzing cement, fly ash and slag, we found that the binding energy of Si_{2p} is related to the activity of cementitious materials; accordingly, lower Si_{2p} binding energy means higher cementitious activity of materials. The maximum binding energy of Si_{2p} is 103.23 eV, and the minimum binding energy of 4.5 h ball-milled slag is 102.67 eV, which shows that the activity of 4.5 h ball-milled slag is the highest, that of 2.5 h ball-milled slag is second and the original slag is lowest (Table 6).

In the Al_{2p} XPS spectra, the peak position shifts in the direction of small-electron-binding energy with the increase in ball-milling time. The electron-binding energy of ball milling 2.5 h slag is the smallest and that of raw slag is the largest; thus, from the binding-energy value, it can be concluded that the aluminum in the raw slag is mainly in the state of six-coordination, and the aluminum in the ball-milled CGS is mainly in the form of the aluminum–oxygen tetrahedron, which shows that the bond structure in the CGS has been changed by the action of mechanical force, and the change of binding energy increases the activity of slag. In minerals, silicon and aluminum exist mainly in the structure of silicon–oxygen and aluminum–oxygen tetrahedra. The change in the binding energy of silicon and aluminum results mainly from the polarization of silicon and aluminum by oxygen, during which the binding energy of oxygen also changes. The changing trend of the binding energy of oxygen, which is the same as that of silicon and aluminum, may reflect CGS activity enhanced by mechanical action, and that activity increases with the duration of mechanical action (Table 6).

The reactivity of material attributes to its high surface [40–42], The activity of cementitious materials also is higher with higher Ca content on the surface of the samples. According to the XPS spectra, the peak area of Ca_{2p} and the content of Ca_{2p} on the surface increased with grinding time, which indicated that the degree of Ca^{2+} participating in hydration reactions had increased. Apparently, mechanical activation can promote CGS gelling activity. The regularity of the surface electron-binding energy of O_{1s}, Si_{2p}, Al_{2p} and Ca_{2p} orbitals before and after CGS activation shows that the activation can change the CGS mineral structure. A decrease in binding energy indicates a lower degree of aggregation of minerals, presumably owing to the mineral structure's becoming unstable, with an increase in surface reactivity. This interpretation is consistent with XRD and FTIR analysis before and after CGS activation.

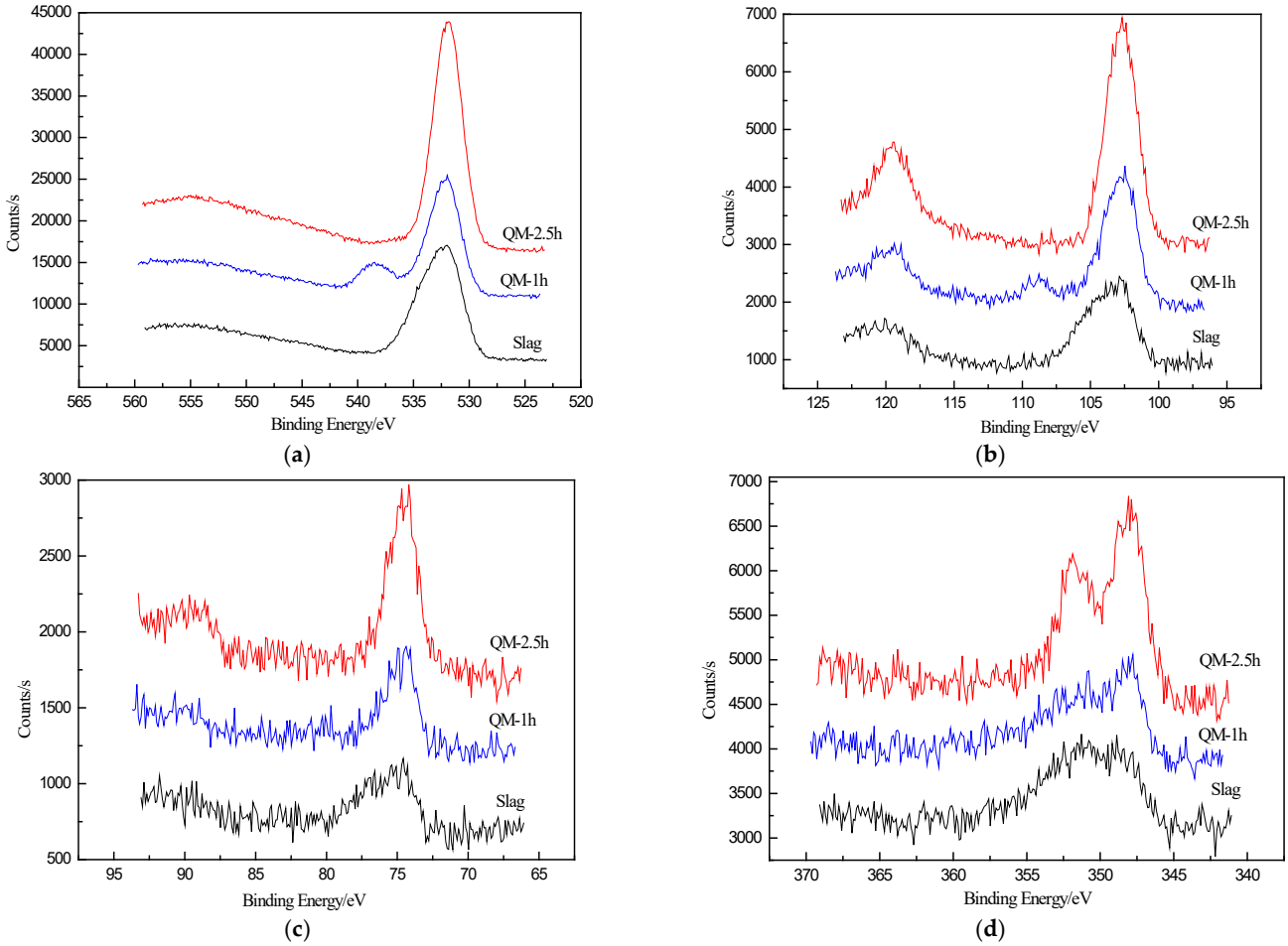

Figure 6. X-ray photoelectron spectrometry diagram of four elements of slag activated by QM methods: O_{1s}, Si_{2p}, Al_{2p} and Ca_{2p}. (**a**) XPS Spectra of O_{1s}; (**b**) XPS Spectra of Si_{2p}; (**c**) XPS Spectra of Al_{2p}; (**d**) XPS Spectra of Ca_{2p}.

Table 6. Electron-binding Energies of Different Elements in Studied Samples.

Electronic Binding Energies	Element			
	O_{1s}	Si_{2p}	Al_{2p}	Ca_{2p}
QM-2.5 h	531.91	102.67	74.48	348.04
QM-1 h	532.12	102.71	74.49	348.06
Slag	532.31	103.23	74.86	350.56

4. Activity Index of Cementitious Materials Prepared from Activated Slag

The composite cementitious materials used in this study were prepared by mixing activated slag and cement in a 7:3 ratio and using a water–cement ratio of 2:5. By analyzing and characterizing the mechanical and microcosmic properties of the composite cementitious block, we explored the effect of activated CGS on the hydration process of the composite system and determined the optimum process of generating composite cementitious material, thereby providing a reliable way for the application of CGS.

According to the comparative analysis of the strength of samples subjected to different grinding methods (Figure 7), the hydration effect of the system with ball-milled CGS is the worst, while the hydration effect of the system with vibration-milled CGS is the best (and its activity index is higher). For the QM-2.5 h block, the compressive strength of the block had decreased by 35.16%, 24.69% and 18.89% by the ages 3 d, 7 d and 28 d, respectively, and for QM-1 h specimen, the compressive strength was 43.23%, 36.90% and 17.67% lower by the ages 3 d, 7 d and 28 d, respectively, than that of cement paste. The difference in

compressive strength between the composite cementitious block and the pure cement block was decreasing; the strength of ZD-2 h and ZY-2 min samples even exceeded that of pure-cement samples after hydration for 28 d. The activity index of ZD-2 h and ZY-2 min samples were 123.2% and 114.6% (Table 7), respectively.

Previous studies have shown that the reactivity of materials increases (characterized by increasing the mechanical strength of geopolymers) [43–46]. The results of this study confirmed that the reactivity of CGS was greatly enhanced in particle size. When the median size (D_{50}) decreases to less than 10 μm, the geopolymer strength tends to increase. The early low strength and late high strength of the composite cementitious block may be due to the activity effect and microaggregate effect of CGS. As the activated CGS was used as cementitious material to replace part of the cement, the clinker mineral content of the composite cementitious system decreased. Early hydration of the system was less than that of a pure-cement system. The pozzolanic activity of activated slag was fully stimulated in the alkaline environment formed by hydration of the cement, and the reaction between the calcium dihydroxide so formed and the activated SiO_2 and Al_2O_3 dissolved by activated CGS promoted the secondary hydration of the cement. However, because the particle size of the activated CSG was smaller than that of cement, it could develop good particle gradation with cement and fill the gap between cement particles. This improved the densification of the composite cementitious system before hydration, and, at a later stage, the strength of the block was also improved.

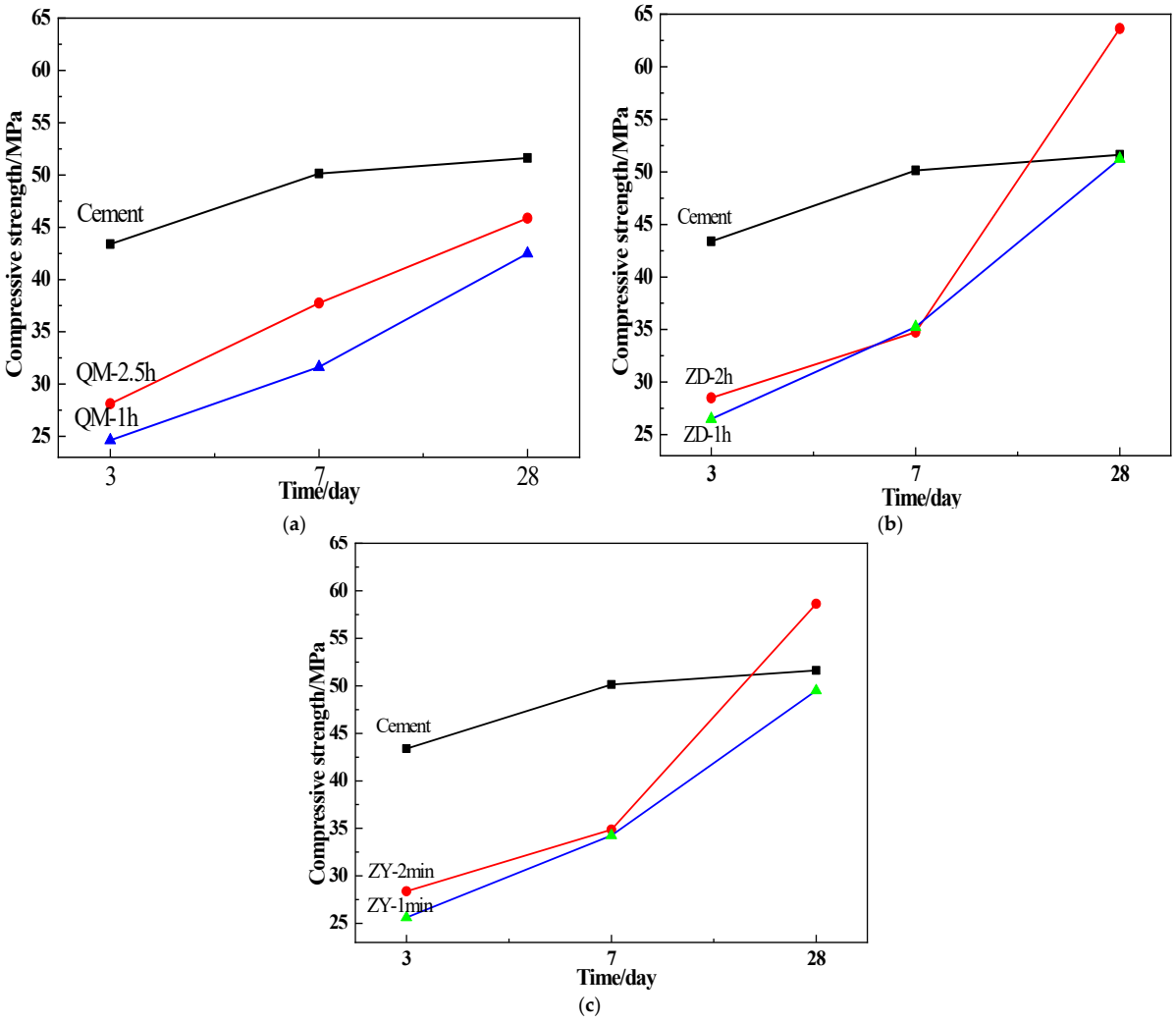

Figure 7. Mechanical properties of composite cementitious materials activated by different grinding methods. (**a**) QM; (**b**) ZD; (**c**) ZY.

Table 7. Dissolution Rate of Activated Silica and Aluminum in Different Activated Slags.

Grinding Mode	Activity Index/%		
	3 d	**7 d**	**28 d**
Cement	100	100	100
QM-2.5 h	64.8	75.3	88.9
QM-1 h	56.8	63.1	82.3
ZD-2 h	65.7	69.3	123.2
ZD-1 h	61.1	70.3	99.3
ZY-2 min	65.4	69.6	114.6
ZY-1 min	59.1	68.3	95.9

Thus overall, the specific surface area of powder particles can be improved, the particle size reduced, the complete crystal structure of powder particles was broken and the degree of crystallization of slag reduced. Furthermore, the surface energy of Si, Al, Ca and other effective elements can be improved and the dissolution of active SiO_2 and Al_2O_3 enhanced through mechanical activation. In summary, the CGS can be used as cement admixture.

5. Conclusions

In this study, the properties of CGS activated by three different mechanical methods were investigated, and the feasibility of using mechanically activated slag as cementitious material was researched by experiment. Our findings support the application of CGS in cement and concrete. The results of our experiments are as follows:

1. There are significant differences in particle-size distribution, mineral composition, degree of crystallinity, particle morphology, chemical bond, surface activity and binding energy, anionic-polymerization degree and hydration properties resulting from three types of grinding.
2. We found that three different mechanical-activation methods could change the internal structure of CGS and improve its gelling activity to different degrees at the same level of particle fineness. We also confirmed that CGS activated by vibration milling and by a prototype grinding machine have the same activity as that by ball milling, and in all three, CGS activity increases with duration of grinding.
3. Mechanical-grinding action reduced the degree of polymerization of [SiO_4] and [AlO_6], and with longer grinding time, the action effect became more significant. The 3-d, 7-d and 28-d strength of CGS paste after mechanical grinding improved significantly, and 28-d activity index of the CGS reached 88.9%, 123.2% and 114.6%, respectively.
4. To sum up, although all three kinds of mechanically activated slags can be used as secondary cementitious materials in cement and concrete, considering the activity index, the grinding power and consumption of materials, the best plan appears to be to replace 30% cement with activated slag as a secondary cementitious material. It can meet the requirement of strength, reduce the amount of cement, reduce the cost and improve the comprehensive utilization ratio of CGS.

Author Contributions: Conceptualization, Funding acquisition, F.W.; Methodology, Writing—review & editing, H.L.; Formal analysis, Investigation, K.Y. All authors have read and agreed to the published version of the manuscript.

Funding: This research was funded by National Natural Science Foundation of China, grant number Z20180222, Independent Research and Development project of State Key Laboratory of Green Building in Western China, grant number LSZZ202021 and Natural Science Foundation of Shaanxi Provincial Department of Education, grant number 20JY041 and Qingyuan Science and Technology Plan Project, grant number 2020KJJH040.

Institutional Review Board Statement: Not applicable.

Informed Consent Statement: Not applicable.

Data Availability Statement: All data included in this study are available upon request by contact with the corresponding author.

Acknowledgments: We acknowledge financial supports by National Natural Science Foundation of China (Z20180222), Independent Research and Development project of State Key Laboratory of Green Building in Western China (LSZZ202021) and Natural Science Foundation of Shaanxi Provincial Department of Education (20JY041) and Qingyuan Science and Technology Plan Project (2020KJJH040).

Conflicts of Interest: The authors declare that there is no conflict of interest in this manuscript.

References

1. Pan, C.; Liang, Q.; Guo, X.; Dai, Z.; Liu, H.; Gong, X. Characteristics of different sized slag particles from entrained-flow coal gasification. *Energy Fuel* **2016**, *30*, 1487–1495. [CrossRef]
2. Ratafia-Brown, J.A.; Manfredo, L.M.; Hoffmann, J.W.; Ramezan, M.; Stiegel, G.J. In an environmental assessment of IGCC power systems. In *Nineteenth Pittsburgh Coal Conference*; University of Pittsburgh: Pittsburgh, PA, USA, 2002; p. 200216.
3. *Gasification Markets and Technologies-Present and Future an Industry Perspective*; US Department of Energy: Washington, DC, USA, 2002; p. 100.
4. Wu, T.; Gong, M.; Lester, E.; Wang, F.; Zhou, Z.; Yu, Z. Characterisation of residual carbon from entrained-bed coal water slurry gasifiers. *Fuel* **2007**, *86*, 972–982. [CrossRef]
5. Wu, S.Y.; Huang, S.; Ji, L.Y.; Wu, Y.Q.; Gao, J.S. Structure characteristics and gasification activity of residual carbon from entrained-flow coal gasification slag. *Fuel* **2014**, *122*, 67–75. [CrossRef]
6. Li, Z.Z.; Zhang, Y.Y.; Zhao, H.Y.; Chen, H.X.; He, R. Structure characteristics and composition of hydration products of coal gasification slag mixed cement and lime. *Constr. Build. Mater.* **2019**, *213*, 265–274. [CrossRef]
7. Wu, S.; Huang, S.; Wu, Y.; Gao, J. Characteristics and catalytic actions of inorganic constituents from entrained-flow coal gasification slag. *J. Energy Ins.* **2015**, *88*, 93–103. [CrossRef]
8. Duan, W.; Yu, Q.; Liu, J.; Hou, L.; Xie, H.; Wang, K.; Qin, Q. Characterizations of the hot blast furnace slag on coal gasification reaction. *Appl. Therm. Eng.* **2016**, *98*, 936–943. [CrossRef]
9. Zhao, X.; Zeng, C.; Mao, Y.; Li, W.; Peng, Y.; Wang, T.; Eiteneer, B.; Zamansky, V.; Fletcher, T. The surface characteristics and reactivity of residual carbon in coal gasification slag. *Energy Fuels* **2010**, *24*, 91–94. [CrossRef]
10. Wagner, N.J.; Matjie, R.H.; Slaghuis, J.H.; Van Heerden, J.H.P. Characterization of unburned carbon present in coarse gasification ash. *Fuel* **2008**, *87*, 683–691. [CrossRef]
11. Xu, S.Q.; Zhou, Z.J.; Gao, X.X.; Yu, G.S.; Gong, X. The gasification reactivity of unburned carbon present in gasification slag from entrained-flow gasifier. *Fuel Process. Technol* **2009**, *90*, 1062–1070. [CrossRef]
12. Acosta, A.; Iglesiasa, I.; Ainetoa, M.; Romero, M.; Rincón, J.M. Utilisation of IGCC slag and clay steriles in soft mud bricks (by pressing) for use in building bricksmanufacturing. *Waste Manag.* **2002**, *22*, 887–891. [CrossRef]
13. Aineto, M.; Acosta, A.; Rincón, J.M.; Romero, M. Production of Lightweight Aggregates from Coal Gasification Fly Ash and Slag. *World Coal Ash* **2005**, 11–15.
14. Yoshitaka, I. Utilization of coal gasification slag collected from IGCC as fine aggregate for concrete. In Proceedings of the EUROCOALASH Conference, Thessaloniki, Greece, 25–27 September 2012.
15. Martin, I.; Echeveria, A.A.; Garcia-Romero, E. Recycling of residual IGCC slags and their benefits as degreasers in ceramics. *J. Environ. Manag.* **2013**, *129*, 1–8. [CrossRef]
16. Masafumi, K.; Reiji, T.; Takao, E.; Shigemi, N. Utilization of the gasification-melting slag from municipal solid waste as fine aggregate for concrete, Concr. *Res. Technol.* **2002**, *13*, 89–98.
17. Pomykala, R. The mechanical properties of coal gasification slag as a component of concrete and binding mixtures. *Pol. J. Environ. Stud.* **2014**, *23*, 1403–1406.
18. Maghool, F.; Arulrajah, A.; Horpibulsuk, S.; Du, Y. Laboratory evaluation of ladle furnace slag in unbound pavement-base/subbase applications. *J. Mater. Civ. Eng.* **2017**, *29*, 1–9. [CrossRef]
19. Maghool FArulrajah, A.; Du, Y.; Horpibulsuk, S.; Chinkulkijniwat, A. Environmental impacts of utilizing waste steel slag aggregates as recycled road construction materials. *Clean Technol. Environ.* **2016**, *19*, 949–958. [CrossRef]
20. Arulrajah, A.; Mohammadinia, A.; Phummiphan, I.; Horpibulsuk, S.; Samingthong, W. Stabilization of recycled demolition aggregates by geopolymers comprising calcium carbide residue, fly ash and slag precursors. *Constr. Build. Mater.* **2016**, *114*, 864–873. [CrossRef]
21. Mohammadinia, A.; Arulrajah, A.; Sanjayan, J.; Disfani, M.M.; Bo, M.W.; Darmawan, S. Stabilisation of demolition materials for pavement base/subbase applications using fly-ash and slag geopolymers: Laboratory investigation. *J. Mater. Civ. Eng.* **2016**, *28*, 1–9. [CrossRef]
22. Heidrich, C.; Ward, C.; Chalmers, D.; Heeley, P.; Ness, J.; Williams, R. Production and handling of coal combustion products. In *Coal Combustion Products Handbook*, 2nd ed.; Ward, C., Heidrich, C., Yeatman, O., Eds.; Ash Development Association of Australia: Port Kembla, Australia, 2014; pp. 1–33.
23. Suryanarayana, C. Mechanical alloying and milling. *Prog Mater. Sci.* **2001**, *46*, 1–184. [CrossRef]

24. Hewitt, S.A.; Kibble, K.A. Effects of ball milling time on the synthesis and consolidation of nanostructured WC–Co composites. *Int J. Refract. Met. Hard Mater.* **2009**, *27*, 937–948. [CrossRef]
25. Sharafi, S.; Gomari, S. Effects of milling and subsequent consolidation treatment on the microstructural properties and hardness of the nanocrystalline chromium carbide powders. *Int. J. Refract. Met. Hard Mater.* **2012**, *30*, 57–63. [CrossRef]
26. Lee, J.S.; Choi, M.S.; Hung, N.V.; Kim, Y.S.; Kim, I.W.; Park, E.C. Effects of high energy ball-milling on the sintering behavior and piezoelectric properties of PZT based ceramics. *Ceram. Int.* **2007**, *33*, 1283–1286. [CrossRef]
27. Razmjou, A.; Mansouri, J.; Chen, V. The effects of mechanical and chemical modification of TiO_2 nanoparticles on the surface chemistry, structure and fouling performance of PES ultrafiltration membranes. *J. Membr. Sci.* **2011**, *378*, 73–84. [CrossRef]
28. Patil, A.G.; Anandhan, S. Ball milling of class-F Indian Fly ash obtained froma thermal power station. *Int. J. Energy Eng.* **2012**, *2*, 57–62.
29. Sharma, A.; Srivastava, K.; Devra, V.; Rani, A. Modification in properties of fly ash through mechanical and chemical activation. *Am. Chem. Sci. J.* **2012**, *2*, 177–187. [CrossRef]
30. Akcay KSirkecioğlu, A.; Tatlıer, M.; Savaşcı, Ö.T.; Erdem-Şenatalar, A. Wet ball milling of zeolite HY. *Powder Technol.* **2004**, *142*, 121–128. [CrossRef]
31. Watanabe, H. Critical rotation speed for ball-milling. *Powder Technol.* **1999**, *104*, 95–99. [CrossRef]
32. Patil, A.G.; Shanmugharaj, A.M.; Anandhana, S. Interparticle interactions and lacunarity of mechano-chemically activated fly ash. *Powder Technol.* **2015**, *272*, 241–249. [CrossRef]
33. Zhao, J.H.; Wang, D.M.; Liao, S.C. Effect of mechanical grinding on physical and chemical characteristics of circulating fluidized bed fly ash from coal gangue power plant. *Constr. Build. Mater.* **2015**, *101*, 851–860. [CrossRef]
34. Kumar, S.; Kumar, R.; Alex, T.C.; Bandopadhyay, A.; Mehrotra, S.P. Effect of mechanically activated fly ash on the properties of geopolymer cement. In Proceedings of the 4th world congress geopolymer, Saint-Quentin, France, 28 June–1 July 2005; pp. 113–116.
35. Arjuan, P.; Silbee, M.R.; Roy, D.M. Quantitative determination of the crystalline and amorphous phases in low calcium fly ashes. In Proceedings of the 10th International Congress of the Chemistry of Cement, Gothenburg, Sweden, 2–6 June 1997; pp. 2–6.
36. Zhang, Q.; Saito, F. A review on mechanochemical synthesis of functional materials. *Adv. Powder Technol.* **2012**, *23*, 523–531. [CrossRef]
37. Fu, X.; Li, Q.; Zhai, J.; Sheng, G.; Li, F. The physical–chemical characterization of mechanically-treated CFBC fly ash. *Cem Concr Compos.* **2008**, *30*, 220–226. [CrossRef]
38. Ding, P.; Orwa, M.G.; Pacek, A.W. De-agglomeration of hydrophobic and hydrophilic silica nano-powders in a high shear mixer. *Powder Technol* **2009**, *195*, 221–226. [CrossRef]
39. Sakthivel SKrishnan, V.V.; Pitchumani, B. Influence of suspension stability on wet grinding for production of mineral nanoparticles. *Particuology* **2008**, *6*, 120–124. [CrossRef]
40. Zhang, J.; Cui, H.; Wang, B.; Li, C.; Zhai, J.; Li, Q. Preparation and characterization of fly ash cenospheres supported CuO–$BiVO_4$ heterojunction composite. *Appl. Surf. Sci.* **2014**, *300*, 51–57. [CrossRef]
41. Oliveira, R.C.; Hammer, P.; Guibal, E.; Taulemesse, J.M.; Garcia, O., Jr. Characterization of metal–biomass interactions in the lanthanum (III) biosorption on Sargassum sp. using SEM/EDX, FTIR, and XPS: Preliminary studies. *Chem. Eng. J.* **2014**, *239*, 381–391. [CrossRef]
42. Huang, Z.Q.; Yi, S.H.; Chen, H.X.; He, X.Q. Parameter analysis of damaged region for laminates with matrix defects. *J. Sandw. Sructures Mater.* **2019**, *23*, 580–620. [CrossRef]
43. Kumar, S.; Kumar, R. Mechanical activation of fly ash: Effect on reaction, structure and properties of resulting geopolymer. *Ceram. Int.* **2011**, *37*, 533–541. [CrossRef]
44. Kumar, S.; Kumar, R.; Alex, T.C.; Bandopadhyay, A.; Mehrotra, S.P. Influence of reactivity of fly ash on geopolymerization. *Adv. Appl. Ceram.* **2007**, *106*, 120–127. [CrossRef]
45. Komljenović, M.; Baščarević, Z.; Bradić, V. Mechanical and microstructural properties of alkali-activated fly ash geopolymers. *J. Hazard. Mater.* **2010**, *181*, 35–42. [CrossRef]
46. Gholipour, G.; Zhang, C.; Mousavi, A.A. Numerical analysis of axially loaded RC columns subjected to the combination of impact and blast loads. *Eng. Struct.* **2020**, *219*, 110924. [CrossRef]